AGU PUBLICATIONS

JGR

Journal of Geophysical Research: Atmospheres

RESEARCH ARTICLE
10.1002/2016JD025834

Key Points:
- Power and momentum flux spectra in a wide-frequency range were estimated using MST radar observations in the Antarctic mesosphere
- Mesospheric wind spectra obey power laws at frequencies higher than the inertial frequency and have isolated peaks at 1 d and at 0.5 d
- Vertical profiles of momentum fluxes show significant eastward forcing, consistent with the mean eastward wind shear and equatorward flow

Correspondence to:
K. Sato,
kaoru@eps.s.u-tokyo.ac.jp

Citation:
Sato, K., M. Kohma, M. Tsutsumi, and T. Sato (2017), Frequency spectra and vertical profiles of wind fluctuations in the summer Antarctic mesosphere revealed by MST radar observations, *J. Geophys. Res. Atmos.*, *122*, 3–19, doi:10.1002/2016JD025834.

Received 28 AUG 2016
Accepted 4 DEC 2016
Accepted article online 9 DEC 2016
Published online 3 JAN 2017

Frequency spectra and vertical profiles of wind fluctuations in the summer Antarctic mesosphere revealed by MST radar observations

Kaoru Sato[1], Masashi Kohma[1], Masaki Tsutsumi[2], and Toru Sato[3]

[1]Department of Earth and Planetary Science, University of Tokyo, Tokyo, Japan, [2]National Institute of Polar Research and The Graduate University for Advanced Studies (SOKENDAI), Tachikawa, Japan, [3]Department of Communications and Computer Engineering, Kyoto University, Kyoto, Japan

Abstract Continuous observations of polar mesosphere summer echoes at heights from 81–93 km were performed using the first Mesosphere-Stratosphere-Troposphere/Incoherent Scatter radar in the Antarctic over the three summer periods of 2013/2014, 2014/2015, and 2015/2016. Power spectra of horizontal and vertical wind fluctuations, and momentum flux spectra in a wide-frequency range from $(8\ \mathrm{min})^{-1}$ to $(20\ \mathrm{days})^{-1}$ were first estimated for the Antarctic summer mesosphere. The horizontal (vertical) wind power spectra obey a power law with an exponent of approximately −2 (−1) at frequencies higher than the inertial frequency of $(13\ \mathrm{h})^{-1}$ and have isolated peaks at about 1 day and a half day. In addition, an isolated peak of a quasi-2 day period is observed in the horizontal wind spectra but is absent from the vertical wind spectra, which is consistent with the characteristics of a normal-mode Rossby-gravity wave. Zonal (meridional) momentum flux spectra are mainly positive (negative), and large fluxes are observed in a relatively low-frequency range from $(1\ \mathrm{day})^{-1}$ to $(1\ \mathrm{h})^{-1}$. A case study was performed to investigate vertical profiles of momentum fluxes associated with gravity waves and time mean winds on and around 3 January 2015 when a minor stratospheric warming occurred in the Northern Hemisphere. A significant momentum flux convergence corresponding to an eastward acceleration of ~200 $\mathrm{m\ s^{-1}\ d^{-1}}$ was observed before the warming and became stronger after the warming when mean zonal wind weakened. The strong wave forcing roughly accorded with the Coriolis force of mean meridional winds.

1. Introduction

Polar mesosphere summer echoes (PMSE) are extremely strong echoes observed by radars located in high latitudes and operated with a wide range of frequency from ultrahigh frequency (UHF) to high frequency (HF). Since the first report of PMSE [*Ecklund and Balsley*, 1981], a number of studies regarding PMSE have been published that demonstrated their seasonality, aspect sensitivity [*Smirnova et al.*, 2012], spectral shape [*Strelnikova and Rapp*, 2011], dependence on geometric and magnetic latitude [*Swarnalingam et al.*, 2009], altitude [*Ecklund and Balsley*, 1981], local time [*Hoffmann et al.*, 1999; *Latteck et al.*, 2007], and the central frequency of the radar (see *Rapp and Lübken* [2004] for a review). While previous studies of PMSE conducted in the 1990s were based mainly on VHF radar observations at high northern latitudes, and with a few at midlatitudes, the number of publications on PMSE in the Southern Hemisphere (SH) has increased recently [*Woodman et al.*, 1999; *Morris et al.*, 2004; *Hosokawa et al.*, 2005; *Kirkwood et al.*, 2007; *Sato et al.*, 2014]. These studies showed that the austral PMSE have similar characteristics to those in the Northern Hemisphere (NH), although the occurrence frequency and central altitude differ slightly.

The overall mechanism of the PMSE is considered as in the following [*Cho and Röttger*, 1997; *Rapp and Lübken*, 2004; *Rapp et al.*, 2008]. Strong echoes result from the coherent scattering that occurs when the electromagnetic fields have structures at the Bragg scale (i.e., a half of wavelength of radio wave which is a few meters for the VHF range for a monostatic radar). Under the atmospheric condition around the polar mesopause during summer, however, turbulence alone cannot explain the existence of small-scale structures satisfying the Bragg condition since turbulence energy dissipates in the viscous subrange during the forward energy cascade. The Bragg condition can be satisfied when Schmidt number (equal to ratio of the kinematic viscosity to the electron diffusion coefficient) becomes larger. In the summer polar mesopause region electrons interact with negatively charged ice particles (or dust) by Coulomb force, and their diffusivity is significantly reduced. The ice particles are observed as polar mesospheric clouds (PMC) by satellites and as noctilucent clouds by ground-based observation instruments. The low diffusivity of electrons hence enables turbulence energy to

cascade to the Bragg scale and can keep the small-scale structures in electron number density perturbations for a significant amount of time after the end of neutral air turbulence [*Rapp and Lübken*, 2003]. Due to the long diffusive time scale, PMSE may emerge even after turbulence in neutral gas disappears. In the height region well above 90 km, however, PMSE are very hard to be created even with the existence of charged ice particles because of increasing kinematic viscosity with increasing height [e.g., *Lübken et al*., 2014].

While PMSE themselves are unique and interesting phenomena in the mesosphere, various information around the mesopause height can be deduced from PMSE observations, e.g., gravity wave characteristics [*Hoffmann et al*., 2008; *Stober et al*., 2013], electron density [*Swarnalingam et al*., 2009; *Varney et al*., 2011], altitude dependence of turbulence [*Smirnova et al*., 2012], and dust particles by HF heating experiments [*Chilson et al*., 2000; *Rapp and Lübken*, 2000; *Havnes*, 2004; *Kassa et al*., 2005]. Atmospheric wave properties are an essential factor for understanding the residual mean circulation in the mesosphere, which is determined approximately by the balance between the Coriolis force and momentum deposition by gravity waves [e.g., *Holton*, 1983; *Watanabe et al*., 2008; *Becker*, 2012; *Placke et al*., 2015].

Becker and Schmitz [2003] and subsequent studies suggest a possible interhemispheric coupling via modulation of propagation and breaking levels of planetary waves and gravity waves [*Becker*, 2012]. Stratospheric planetary wave amplitudes during winter are larger in the NH than those in the SH. Thus, observations of the summer mesosphere in the SH may be more effective for research on the interhemispheric coupling because it is initiated by modulation of the stratosphere by the planetary waves in the winter hemisphere. Modeling studies [*Becker and Fritts*, 2006; *Körnich and Becker*, 2010] and observations of PMC brightness by satellites [*Karlsson et al*., 2009] also support the connection between the NH winter stratosphere and the SH summer mesosphere. Recently, *Murphy et al*. [2012] examined 17 year mesospheric wind observations by the MF radar at Davis Station (68.6°S, 78.0°E) and the UKMO reanalysis data in January and showed that the response of mesospheric meridional winds to the stratospheric perturbations in the NH strongly depends on the phase of the quasi-biennial oscillation in the equatorial stratosphere. They also noted that the cross-equator response of temperature does not necessarily accord with the mechanism proposed by *Becker and Fritts* [2006]. According to *Yasui et al*. [2016], who examined 15 year observations of horizontal winds by the MF radar at Syowa Station (69.00°S, 39.35°E), the relationship between wind variances associated with mesospheric gravity waves in the SH and a sudden stratospheric warming (SSW) in the NH is not statistically significant, at least not over Syowa Station. Therefore, while the existence of the interhemispheric coupling phenomenon is widely accepted, the mechanism coupling the stratosphere of one hemisphere to the mesosphere of the other hemisphere is still unclear. Further studies on mesospheric gravity waves in the SH are needed in order to elucidate the mechanism of the interhemispheric coupling in the middle atmosphere.

The PANSY radar is a Mesosphere-Stratosphere-Troposphere/Incoherent Scattering (MST/IS) radar, which was installed at Syowa Station in 2011 [*Sato et al*., 2014]. The PANSY radar has been performing observations of the mesosphere as well as the troposphere and stratosphere. As the PANSY radar currently has the largest power-aperture product (a measure of the MST/IS radar performance) in the Antarctic, PMSE are observed almost continuously in the summer period (usually mid-November through mid-February). In the present study, interannual and intraseasonal variations of wind fluctuation characteristics in the summer Antarctic mesosphere are examined using PMSE observations by the PANSY radar for the three summer seasons of 2013/2014, 2014/2015, and 2015/2016.

It is worth noting that MST radar observations provide accurate estimates of the momentum fluxes associated with gravity waves using the dual-beam method proposed by *Vincent and Reid* [1983] even for the mesosphere. However, MST radar observations for the mid- and low-latitude mesosphere are possible only during the daytime, when the atmosphere is sufficiently ionized by solar radiation. Thus, the momentum flux estimation for the mesosphere is possible but only for a limited high-frequency range of gravity waves at low and middle latitudes [e.g., *Tsuda et al*., 1990]. In contrast, in the polar region, echoes from the mesosphere are almost continuously detected over a few months of the summer season if the radar sensitivity is sufficiently high like the PANSY radar because of continuous solar radiation during the whole day and because of the presence of polar mesospheric clouds [*Rapp and Lübken*, 2003]. Thus, it is possible to estimate the momentum fluxes as well as the wind variance as a function of frequency over a much wider range from $(\text{several minutes})^{-1}$ to $(\text{several 10 days})^{-1}$, including almost the entire gravity wave frequency range. This indicates the value in and uniqueness of the present study.

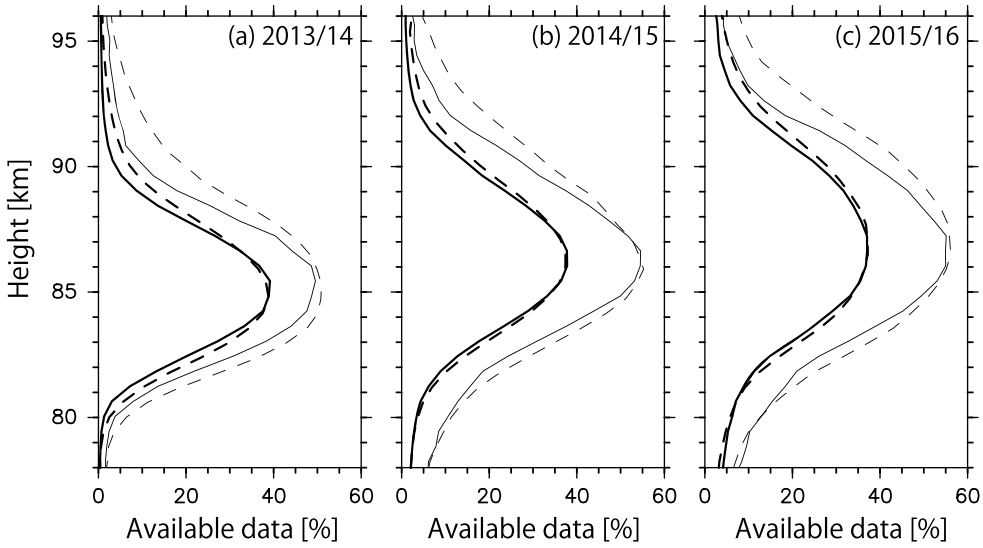

Figure 1. Percentage of available data as a function of height for time periods of 15 November through 20 February in (a) 2013/2014, (b) 2014/2015, and (c) 2015/2016. Solid (dashed) curves for vertical (tilted) beam observations and thick (thin) curves for 1 min (30 min) data.

This study is organized as follows. A description of the data and method of analysis is given in section 2. Polar mesosphere summer echoes observed by the PANSY radar over the 3 years are shown and compared with satellite temperature observations in section 3. Statistical characteristics such as power and momentum flux spectra and vertical profiles of momentum fluxes are examined in section 4. Section 5 gives a case study of the mean wind change and momentum flux divergence associated with gravity waves in early January in 2014/2015 at approximately the time when an SSW occurred in the NH. A summary and concluding remarks are given in section 6.

2. Data Description and Method of Analysis

2.1. PANSY Radar Observations

PMSE data obtained over three summer seasons by routine observations of the PANSY radar, which is located at Syowa Station in the Antarctic (69.00°S, 39.35°E), are mainly analyzed and discussed. The time periods analyzed are 15 November through 20 February in three austral summer seasons of 2013/2014, 2014/2015, and 2015/2016. The time resolution of the PMSE data is approximately 1 min, but the observation time intervals are approximately 3 min and 20 s because of interleaving observations for the troposphere and stratosphere. Five beams are used, which are pointed to the vertical and tilted to the north, east, south, and west with a zenith angle of 10°. The analyzed height range is from 78–96 km with a resolution of 600 m along the beam direction. The top and bottom observable regions depend on the atmospheric condition such as the presence of the polar mesospheric clouds, as described in section 1. Details of the PANSY radar were documented by *Sato et al*. [2014].

Winds are usually estimated from the Doppler shift of the radar echoes by fitting the echo spectra into a Gaussian shape with a least squares method. The accuracy depends mainly on the echo power and on the initial guess for the fitting. Thus, in this study, additional fitting was made for echo spectra integrated over every 30 min in order to reduce the statistical noise. The initial guess used for the fitting for the echo spectra was obtained as a maximal frequency for a sum of the logarithms of the original 1 min echo spectra over 2 h, a duration over which the winds usually do not significantly change. This procedure reduces the contamination from sporadic meteor echoes. Details of the method were described by *Sato et al*. [1997].

Figure 1 shows the percentage of available data from original 1 min echo spectra (thick curves) and from 30 min echo spectra by the above mentioned method (thin curves) as a function of the height for each

summer season. The displayed height level is taken from the ground surface of Syowa Station (15 m above the sea level). Solid (dashed) curves show the results for vertical (tilted) beams. The percentage of data available from the 30 min echo spectra is larger than that from the 1 min echo spectra by 10–20% depending on the height.

The well-observed height range depends on the year, partly because of atmospheric conditions and partly because of the radar system sensitivity. The PANSY radar was operated with a partial 12-group system for 2013/2014 and 2014/2015, while a full-system operation using all 55 groups was performed for 2015/2016. For example, the height range with the percentage of available data larger than 20% from the 1 min echo spectra of the vertical beam is 82.3–88.0 km (a range of 5.7 km) for 2013/2014, 83.2–89.5 km (6.3 km) for 2014/2015, and 82.8–91.0 km (8.2 km) for 2015/2016. The peak of available data percentage is observed at ~85.5 km for 2013/2014, ~86.3 km for 2014/2015, and ~86.5 km for 2015/2016.

The wind data from the 1 min echo spectra are used for the analyses of the power spectra, momentum flux spectra, and vertical profiles of momentum fluxes in section 4. The data from the 30 min echo spectra are used to examine time-height sections of the volume reflectivity of PMSE over the entire analysis period of 15 November through 20 February of each summer in section 3 and a focused period from 20 December 2014 to 20 January 2015 in section 5.

In this study, temperature data from a satellite, Aura Microwave Limb Sounder (MLS) Version 3.3/3.4 Level 2 [*Waters et al.*, 2006], are also used to examine the dependence of the PMSE intensity on the background temperature.

2.2. Method of Analysis

The frequency power spectra and momentum flux spectra were estimated using power spectra of line-of-sight wind fluctuations from five beams following *Sato* [1990], which is an extension of the method proposed by *Vincent and Reid* [1983]. The line-of-sight wind velocities $V_{\pm\theta}$ for the beams tilted to the east and west with a zenith angle of θ are expressed using zonal wind $u_{\pm\theta}$ and vertical wind $w_{\pm\theta}$ as

$$V_{\pm\theta} = \pm u_{\pm\theta} \sin\theta + w_{\pm\theta} \cos\theta \tag{1}$$

Thus, the frequency power spectra $P_{V_{\pm\theta}}(\omega)$ for line-of-sight wind fluctuations for beams tilted to the east and west are expressed using power spectra of $u_{\pm\theta}$ ($P_{u_{\pm\theta}}(\omega)$) and $w_{\pm\theta}$ ($P_{w_{\pm\theta}}(\omega)$), and momentum flux spectra $Re\left[U_{\pm\theta}(\omega)W^*_{\pm\theta}(\omega)\right]$:

$$P_{V_{\pm\theta}}(\omega) = P_{u_{\pm\theta}}(\omega)\sin^2\theta \pm Re\left[U_{\pm\theta}(\omega)W^*_{\pm\theta}(\omega)\right]\sin 2\theta + P_{w_{\pm\theta}}(\omega)\cos^2\theta, \tag{2}$$

where ω is observed frequency, $U_{\pm\theta}(\omega)$ ($W_{\pm\theta}(\omega)$) is a Fourier component of $u_{\pm\theta}$ ($w_{\pm\theta}$) at ω, and asterisk shows its complex conjugate. By assuming that the power spectra and momentum flux spectra are homogeneous between the two beam positions, we obtain

$$Re[U(\omega)W^*(\omega)] = \frac{P_{V_{+\theta}}(\omega) - P_{V_{-\theta}}(\omega)}{2\sin 2\theta}, \tag{3}$$

and

$$P_u(\omega) = \frac{P_{V_{+\theta}}(\omega) + P_{V_{-\theta}}(\omega)}{2\sin^2\theta} - P_w(\omega)\cot^2\theta. \tag{4}$$

Note that $Re[U(\omega)W^*(\omega)]d\omega$ shows contribution by waves in a frequency range between ω and $\omega + d\omega$ to the net momentum flux $\overline{u'w'}$. Power spectra of w fluctuations, $P_w(\omega)$, are directly estimated from line-of-sight velocity of the vertical beam. The heights for which $P_w(\omega)$ are estimated are different from those for $P_{V_{\pm\theta}}(\omega)$ for oblique beams. Thus, a linear interpolation in the vertical is made before calculation using (4). Similarly, $P_v(\omega)$ and $Re[V(\omega)W^*(\omega)]$ are obtained from the two power spectra using line-of-sight wind fluctuations of the beams tilted to the north and south.

It is worth noting that the above mentioned method using the assumption of uniform variance and flux fields at each frequency between the symmetric beams gives better estimates than other methods that require an assumption of a homogeneous wind field between the symmetric beams (i.e., wave phases observed by the symmetric beams are the same) [*Fukao et al.*, 1988; *Sato*, 1990].

3. Polar Mesosphere Summer Echoes Over Three Summer Periods in 2013/2014, 2014/2015, and 2015/2016

The volume reflectivity is determined from the radar equation as follows: The transmitted power is computed from measured output power of individual transmit receive (TR) module. As the output of each TR module is directly fed to each antenna, cable and connector losses are small and well calibrated. The antenna pattern is computed as shown in *Sato et al.* [2014]. The received echo power is calibrated using the galactic noise as a reference [*Guzman et al.*, 2011]. The minimum volume reflectivity with detectability threshold of 3 for the mean galactic noise level averaged for 30 min is $2.4 \times 10^{-16}\,\mathrm{m}^{-1}$ for 2013/2014 and 2014/2015 data, and $3.2 \times 10^{-17}\,\mathrm{m}^{-1}$ for 2015/2016 data. Figure 2 shows time-height sections of volume reflectivity of PMSE on 15 November through 20 February of the next year in each summer season. Here we followed *Kirkwood et al.* [2007] for the occurrence threshold of PMSE at $1 \times 10^{-15}\,\mathrm{m}^{-1}$. PMSE are almost continuously observed by the PANSY radar in all years.

Year-to-year variation of the seasonal evolution of the PMSE is large. Such variation seems attributable to the year-to-year variation of the temperature evolution in the mesosphere. Figure 3 shows the same time-height sections as for Figure 2 but for temperature averaged for 65°S–70°S and for 12°E–60°E near Syowa Station from Aura MLS observations. The late start of the PMSE in 2015 compared with other years corresponds to relatively high temperatures in the last half of November 2015.

Kirkwood et al. [2007] and subsequent studies [e.g., *Lübken et al.*, 2014] indicated that the PMSE detection in the SH usually starts at high altitudes and descends gradually with time. Such a feature is observed in the 2014/2015 and 2015/2016 seasons but not in 2013/2014. Strong volume reflectivity of PMSE even at low altitudes of ~80 km in the early summer season of 2013/2014 seems attributable to quite low temperatures there, as shown in Figure 3a. Possible candidate mechanisms causing such an interannual variation in the summer mesospheric temperature are intrahemispheric and interhemispheric couplings [e.g., *Becker et al.*, 2015; *Lübken et al.*, 2016]. Further studies from this viewpoint are needed based on observations over multiple years.

4. Statistical Characteristics of the Mean Wind and Wind Fluctuations in the Summer Mesosphere

4.1. Spectral Characteristics

4.1.1. Frequency Power Spectra

As stated in section 1, MST radars usually detect echoes only in the daytime in the mesosphere, and hence, the observations are not continuous in low and middle latitudes. In contrast, PMSE are continuously observed in the polar summer mesopause region. Thus, the frequency spectra of horizontal and vertical wind fluctuations in the mesosphere can be obtained over a wide-frequency range, which we performed for the first time using PANSY radar observations. The spectra for u, v, and w fluctuations [$P_u(\omega)$, $P_v(\omega)$, and $P_w(\omega)$], where ω is the angular frequency, are obtained by using the *Blackman and Tukey* [1958]'s method for each height and averaged for a height range from 84 to 88 km where the numbers of missing data are relatively small for all years. Results are shown in Figure 4. The displayed frequency range is from (2π/20 day) to (2π/8 min). This frequency range covers almost the entire frequency range of internal gravity waves which is from the Brunt-Väisälä frequency (about (2π/5 min) in the stratosphere and mesosphere) to the inertial frequency f (about (2π/13 h) at Syowa Station) in the case that the Doppler shift by the mean wind is negligible. Different colors indicate results for different summer seasons, and each spectrum is shifted by one digit to see the detailed structure for each summer.

Spectral shapes are similar for the 3 years for each wind component. At frequencies higher than f, $P_u(\omega)$ and $P_v(\omega)$ are approximately proportional to ω^{-2} and $P_w(\omega)$ to ω^{-1}. Such a power law structure and steep slopes in the higher-frequency region is consistent with previous studies showing results for middle latitudes [e.g., *Muraoka et al.*, 1990]. At frequencies lower than f, the slopes of both horizontal and vertical wind spectra are shallower. In the lower frequency region, there are a few dominant peaks. First, two dominant peaks are observed around a 1 day period and a half-day (or the inertial) period in all spectra. Second, an isolated peak around a 2 day period is observed in $P_u(\omega)$ and $P_v(\omega)$ but is absent in $P_w(\omega)$. These features suggest that the quasi-2 day waves obey different dynamics from disturbances having periods of 1 day and a half day. The peaks around 1 day and half-day periods are likely due to tides and/or inertia-gravity waves which are

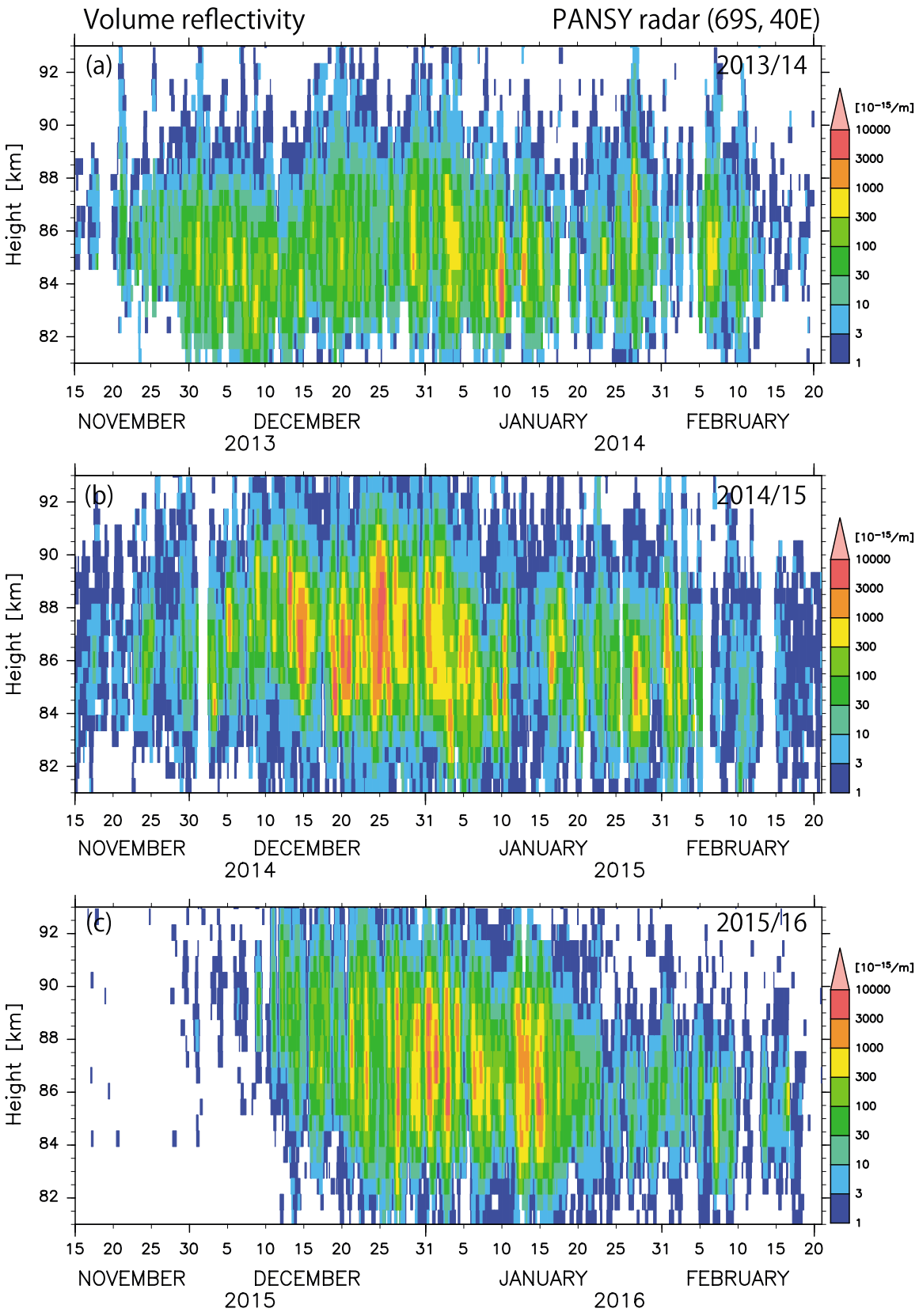

Figure 2. Time-height sections of volume reflectivity of polar mesosphere summer echoes observed by the vertical beam for (a) 2013/2014, (b) 2014/2015, and (c) 2015/2016.

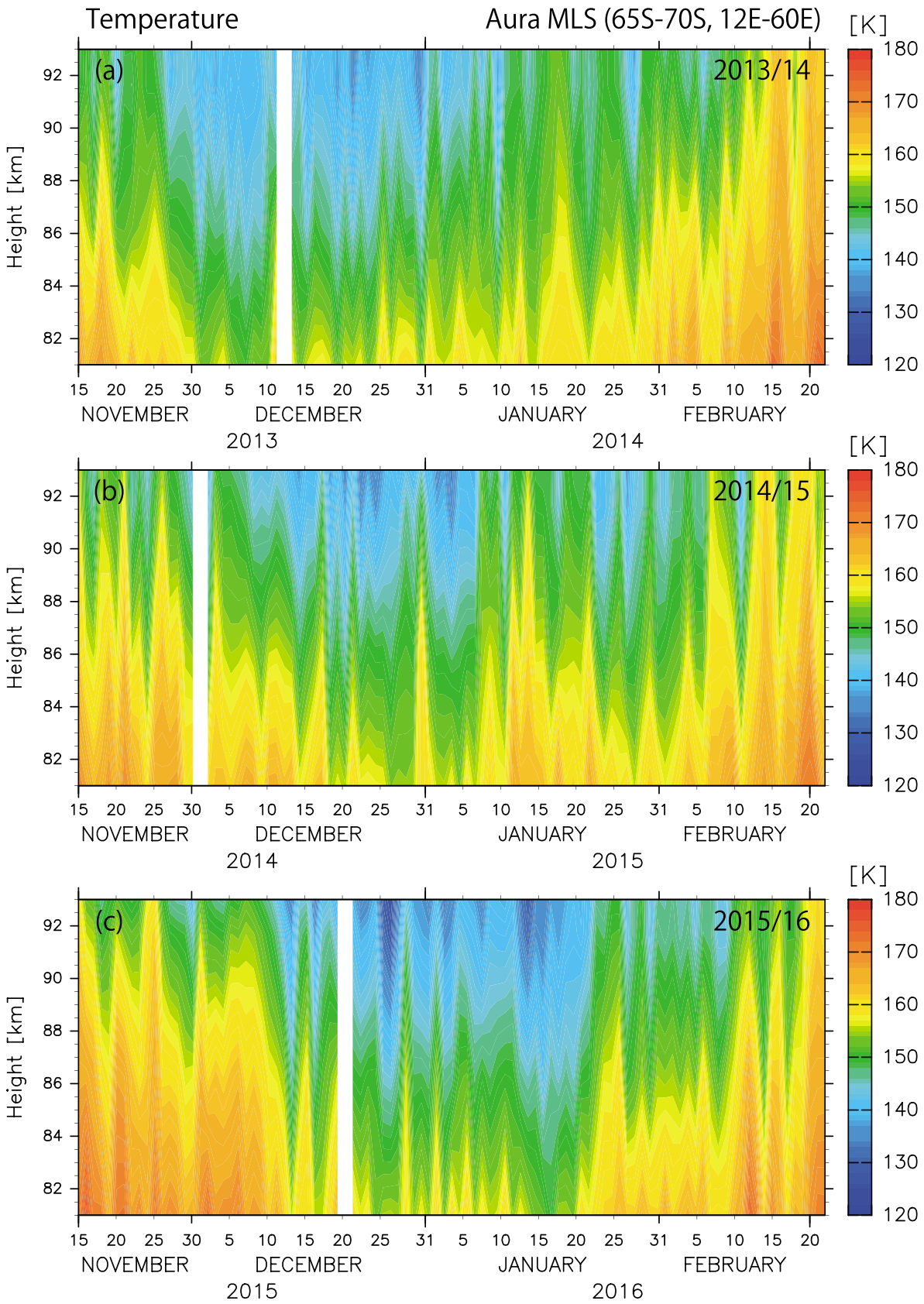

Figure 3. The same as Figure 2 but for temperature from Aura MLS observations averaged for 65°S–70°S and 12°E–60°E.

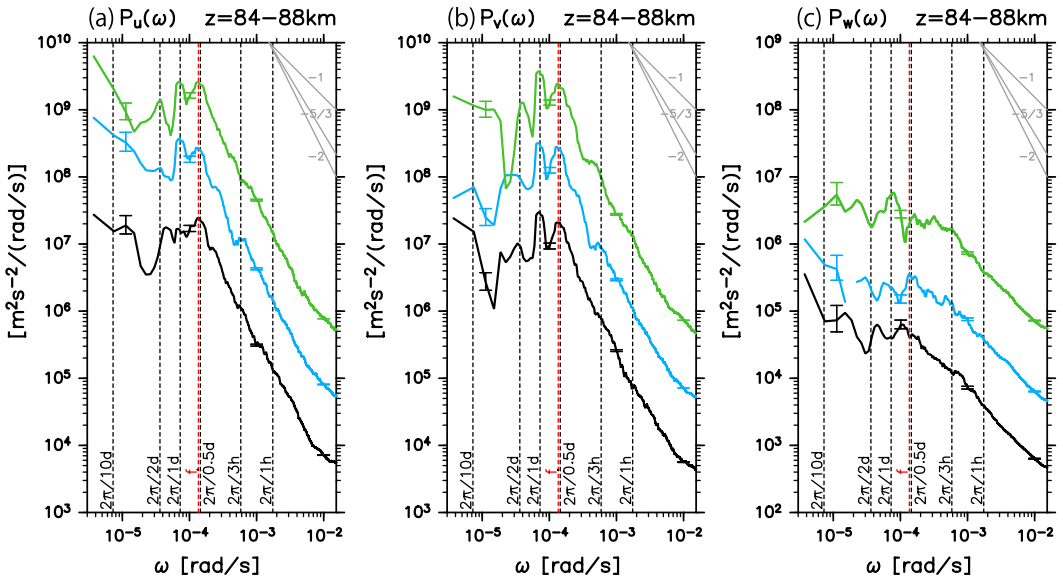

Figure 4. Frequency power spectra of (a) zonal, (b) meridional, and (c) vertical wind fluctuations. The power spectra averaged for the height region of 84–88 km are shown. Black, blue, and green indicate the spectra for 2013/2014, 2014/2015, and 2015/2016, respectively. Gray lines on the upper right corner indicate the slopes of ω^{-1}, $\omega^{-5/3}$, and ω^{-2}. Vertical red dotted line indicates the inertial period, which is ~13 h at observation site (69°S). The spectra for 2014/2015 and 2015/2016 are, respectively, shifted by one and two digits in the vertical. Error bars show intervals of the 99% statistical significance.

characterized as waves with large horizontal divergence (i.e., strong vertical wind components). Previous studies suggest that the quasi-2 day waves that are frequently observed in the mesosphere and lower thermosphere are likely due to a normal-mode Rossby-gravity wave [e.g., *Rodgers and Prata*, 1981; *Salby*, 1981; *Baumgaertner et al*., 2008, and references therein]. The difference in the spectral characteristics around the 2 day period between horizontal and vertical wind components observed in Figure 4 is consistent with this indication (i.e., weak vertical wind components). It is also worth noting that these spectral characteristics are most evident in the spectra for the 2015/2016 season obtained using full-system PANSY radar observations.

Minamihara et al. [2016] showed the power spectra of horizontal and vertical wind fluctuations in the lower troposphere in a frequency range from (2π/20 d) to (2π/8 min) using PANSY radar observations over 3 years. The power spectra of the lower troposphere also obey different power laws between high- and low-frequency ranges. The slopes of tropospheric and mesospheric power spectra of horizontal wind fluctuations [$P_u(\omega)$ and $P_v(\omega)$] are similar for the high-frequency range. However, the transition frequency from the high- to low-frequency regions is approximately (2π/7 d) for the lower troposphere, while it is approximately equal to the inertial frequency f (~2π/13 h) in the mesosphere. This difference is consistent with the Charney and Drazin theorem [1961] indicating that planetary waves having low frequencies originating from the troposphere hardly propagate into the westward wind in the summer stratosphere and above.

In contrast, the transition frequency of $P_w(\omega)$ in the lower troposphere between the low- and high-frequency regions is approximately equal to f which is similar to the mesospheric spectra. In addition, both power law exponents for the low- and high-frequency regions of the lower tropospheric spectra are similar to those of the mesospheric ones. This similarity in the vertical wind spectra between the troposphere and mesosphere is in marked contrast with the differences in the horizontal wind spectra. One plausible explanation is that low-frequency vertical wind fluctuations are dominated by gravity waves, which are largely Doppler shifted by the mean wind, because gravity waves can inherently propagate both in the eastward and westward background winds (unlike planetary waves) unless they encounter their critical levels. For example, gravity waves generated by strong surface winds over steep topography around the coastal region of the Antarctic continent [e.g., *Shibuya et al*., 2015; *Tomikawa et al*., 2015; *Minamihara et al*., 2016] or radiated through resonance with a large-scale balanced flow [*Yasuda et al*., 2015a, 2015b] are those which have such low (ground-based) frequencies.

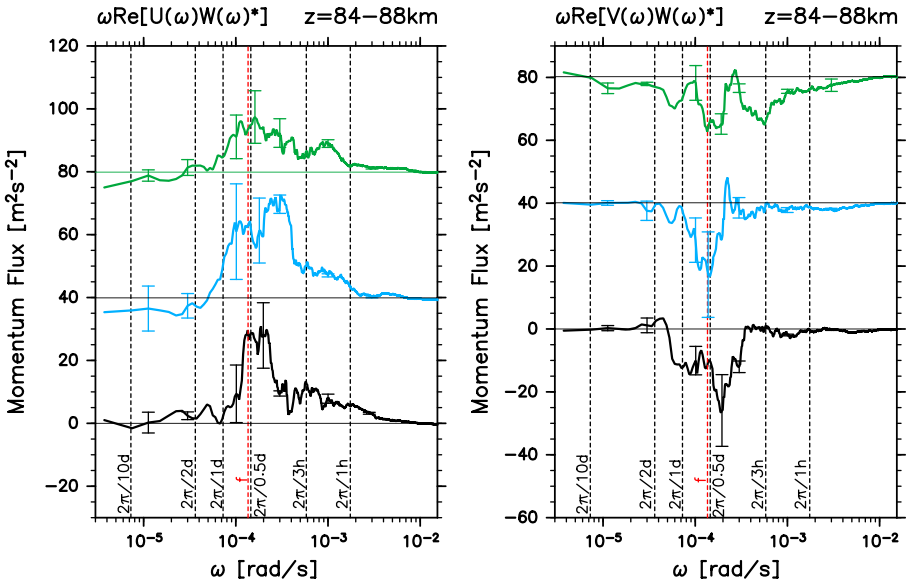

Figure 5. Momentum flux spectra versus frequency averaged for the height region of 84–88 km in a flux content form. (left) $\omega Re[U(\omega)W^*(\omega)]$. (right) $\omega Re[V(\omega)W^*(\omega)]$. Black, blue, and green indicate the spectra for 2013/2014, 2014/2015, and 2015/2016, respectively. The spectra for 2014/2015 and 2015/2016 are, respectively, offset by 50 $m^{-2} s^{-2}$ and 100 $m^{-2} s^{-2}$. Error bars show intervals of the 95% statistical significance.

Note that *Becker and Brune* [2014] suggested using a mechanistic general circulation model (GCM) simulation that the power law shaped spectra may be due to stratified turbulence maintained by primary gravity waves. The origin of the particular power laws in the frequency spectra as found in the present paper is subject to future studies.

4.1.2. Momentum Flux Spectra

Figures 5a and 5b, respectively, show zonal and meridional momentum flux spectra averaged for a height region of 84–88 km where the number of available data is sufficiently large. Different colors indicate the results for different years. It is commonly seen for the 3 years that $Re[U(\omega)W^*(\omega)]$ is mainly positive and $Re[V(\omega)W^*(\omega)]$ is mainly negative. This feature suggests that gravity waves propagating eastward and poleward relative to the mean wind are dominant if they originate from the lower atmosphere and propagate energy upward. The dominance of poleward propagation is consistent with results by *Yasui et al*. [2016] indicating that gravity waves in the summer mesosphere in the Antarctic may originate from tropical convection based on MF radar observations at Syowa Station over 15 years. A numerical experiment and theoretical consideration by *Sato et al*. [1999] and *Sato* [2000] suggested the possibility of such lateral propagation of gravity waves over a long distance.

It is interesting that both momentum fluxes are largely contributed by components with relatively long periods of 1 h $\leq \tau \leq$ 1 day. Contribution by shorter-period (i.e., 8 min $\leq \tau \leq$ 1 h) components is also significant but relatively smaller.

4.2. Vertical Profiles of Mean Wind and Vertical Momentum Fluxes

Convergence of the vertical flux of horizontal momentum gives the wave forcing to the mean wind which is associated with gravity waves having middle and high intrinsic frequencies. The vertical resolution of the PANSY radar observation is sufficient to evaluate such gravity wave forcing. Because planetary waves from the troposphere cannot propagate deep in the westward mean wind, the summer mesosphere may be zonally uniform compared to the winter mesosphere. In addition, the surface winds are generally weak in the summer and thus do not generate strong gravity waves forced by topography which would exhibit large regional variability. Thus, the estimates of vertical momentum flux from the PANSY radar observations may be representative of typical values in the summer high-latitude mesosphere, even though the estimates are based on observations at only one location.

Here it should be noted that observed convergence of the vertical momentum flux gives an upper limit of gravity wave forcing. This is because gravity waves with low intrinsic frequencies also possess a significant Stokes drift, which are attributable to a meridional heat flux part of the vertical component of the Eliassen-Palm (E-P) flux, and resultant E-P flux divergence can be smaller than the momentum flux convergence. See *Miyahara et al*. [1986] for details. Note also that quasi-2 day and 5 day waves, which are in situ generated in the summer mesosphere-lower thermosphere, can produce a significant forcing opposite to the gravity wave forcing [*Becker*, 2012].

Figure 6 shows vertical profiles of U and density-weighted vertical flux of zonal momentum $\rho_0\overline{u'w'}$ (left column) and V and density-weighted vertical flux of meridional momentum $\rho_0\overline{v'w'}$ (right column) averaged over 15 November through 20 February of each year from 2013/2014, 2014/2015, and 2015/2016. Here components with wave periods shorter than 1.5 days which associate with large momentum fluxes (see Figure 5) are designated as fluctuations by primes ($'$). Note that the displayed vertical ranges are different for different years. The vertical profiles for 2015/2016 cover a vertical extent of ~8 km, which is greater than those of the other 2 years (~6 km or less). This is because the PANSY radar observations for this year were performed using its full system.

In all years, U is mainly westward and $\rho_0\overline{u'w'}$ is positive, while V is mainly northward and $\rho_0\overline{v'w'}$ is negative with a limited number of exceptions. The mean zonal wind U decreases with height in all years. However, detailed structure depends on the year. For example, vertical shear in U is larger in 2014/2015 than in 2013/2014. In 2015/2016, the shear is large below 87 km, small in the range of 87–89 km, and large above 89 km. It is interesting that the magnitude of decrease in $\rho_0\overline{u'w'}$ with height seems larger for stronger vertical shear of U. The convergence of the momentum flux $-\frac{1}{\rho_0}\frac{\partial\rho_0\overline{u'w'}}{\partial z}$ is regarded as the gravity wave forcing to the mean zonal wind. For example, the momentum flux convergence is large in 2014/2015 and is ~120 m s^{-1} d^{-1}. This direct estimate of the gravity wave forcing by radar observations is consistent with and hence supports the results from a mechanistic GCM by *Becker* [2012].

The residual mean flow $[v]^*$ in the Transformed Eulerian Mean theory [e.g., *Andrews et al*., 1987], an approximation of the Lagrangian mean flow, is expressed as $[v]+[v]^S$, where [ ] denotes the zonal mean and $[v]^S$ is Stokes drift by waves. The residual mean flow $[v]^*$ in the mesosphere is mainly caused by gravity waves (which are less affected by Earth's rotation) and hence is roughly equal to $[v]$ [*Sato et al*., 2013] which is directly compared with the observation V. In the present case, gravity waves with large momentum fluxes have long periods (see Figure 5) and hence may be affected by Earth's rotation. It should be noted, however, that the wave periods displayed in Figure 5 are ground relative and may be significantly longer than the intrinsic (i.e., relative to the mean wind) wave periods due to a strong Doppler shift by the mean wind. Stokes drift $[v]^S$ due to gravity waves with such short intrinsic periods is negligible. In fact, using the wave forcing of ~120 m s^{-1} d^{-1} for 2014/2015, ignoring $[v]^S$, and hence assuming that the wave forcing should be balanced with Coriolis force $-f[v]$ [*Sato et al*., 2013] yields $[v]\approx 10.4$ m s^{-1}, which is smaller than the observations V (~18 m s^{-1}) (Figure 6) but comparable nonetheless. Note that the difference between $[v]$ and V may be due to the forcing due to other types of waves and/or other nonlinear contributors [*Becker*, 2012].

5. A Case Study on the Relationship of the Momentum Flux Convergence With Change in the Mean Wind in 2014/2015

On 3 January 2015, a strong SSW occurred in the NH [e.g., *Manney et al*., 2015]. Figure 7 shows time-height sections of the PMSE, U, and V observed by the PANSY radar from 20 December 2014 to 21 January 2015. An interesting feature is that U becomes eastward above 88 km in the time period from 4 to 12 January after the SSW occurred. Almost simultaneously, V becomes stronger around 88 km where U is approximately zero. It is theoretically expected that when the level where $U=0$ descends, the level of gravity wave drag should also descend; and hence, the level of strong V, which is balanced with the gravity wave drag, should also descend. The appearance of a strong V layer around 88 km where $U\approx 0$ is consistent with the theoretical expectation.

Note that the response of the SH mesosphere to the NH SSW is usually observed after a time lag of several days depending on the event. Thus, the change before and after the SSW date may not be related to the SSW directly. A direct response to the SSW caused by an interhemispheric coupling [*Körnich and Becker*, 2010] can

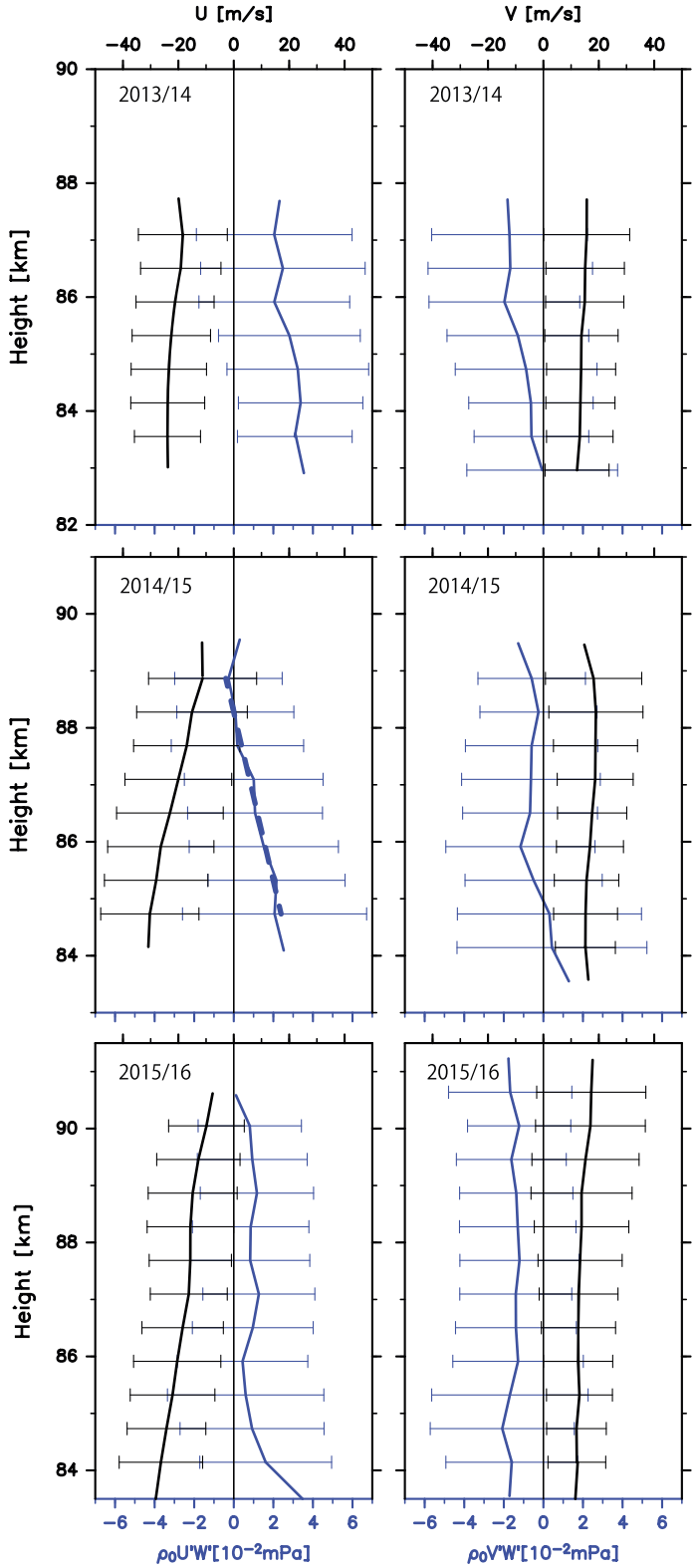

Figure 6. Vertical profiles of time mean (left, black curves) zonal wind, (right, black curves) and meridional wind, and vertical fluxes of (left, blue curves) zonal momentum and (right, blue curves) meridional momentum in austral summer (15 November to 20 February) of 2013/2014 (top row), 2014/2015 (middle row), and 2015/2016 (bottom row). A straight dashed line in Figure 6 (middle left) shows the gradient used for the estimate of momentum flux divergence. Error bars show the standard deviation of wind fluctuations at each height for each summer season.

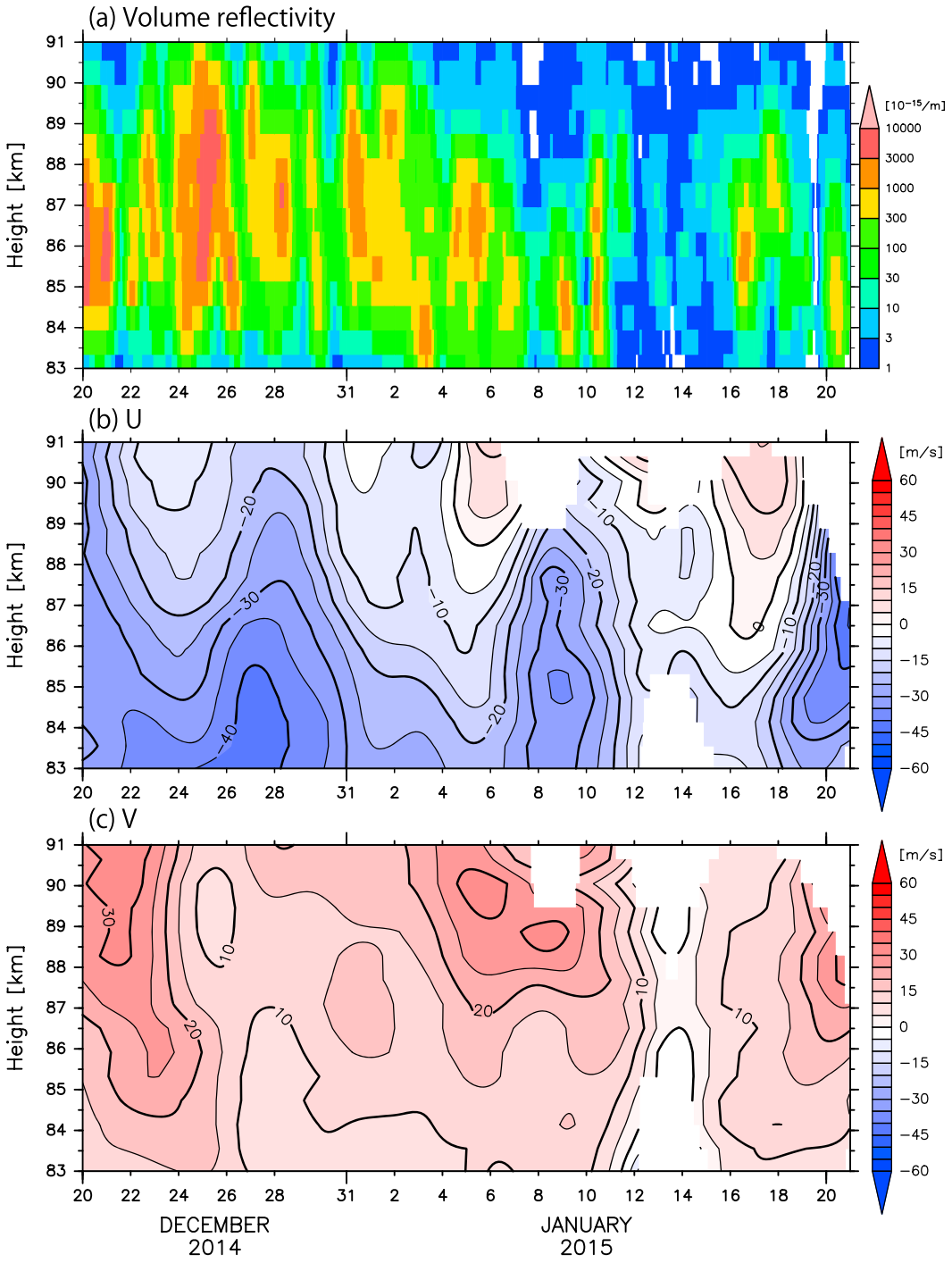

Figure 7. Time-height sections of (top) volume reflectivity obtained from the vertical beam observations, (middle) zonal wind *U*, and (bottom) meridional wind *V* estimated from oblique beams in the time period of 20 December 2014 to 20 January 2015. A low-pass filter with a cutoff length of 5 days was applied for *U* and *V*.

be a warming observed from 12 to 14 January by Aura MLS shown in Figure 3b. This warming in the SH mesosphere is consistent with significantly weak echoes detected by the PANSY radar during the period, suggesting a decrease in the amount of polar mesospheric clouds. Because of the weak echoes, however, it is difficult to estimate the change in the momentum flux convergence and its relationship to change in the mean wind.

We examined change in the momentum flux convergence before and after 3 January 2015 because the interesting changes in U and V were observed as stated above, and because we cannot deny the possibility that the changes occur in response to the NH SSW. A detailed analysis is performed for two time periods over 7 days from 27 December 2014 to 2 January 2015 (hereafter referred to as Period A) and from 4 to 10 January 2015 (Period B).

Figure 8 shows vertical profiles of U and $\rho_0\overline{u'w'}$ (left column) and V and $\rho_0\overline{v'w'}$ (right column) averaged for Period A (top row) and for Period B (bottom row). A significant decrease in positive $\rho_0\overline{u'w'}$ is observed in Period A as shown by a straight dashed line. The convergence of the momentum flux $-\frac{1}{\rho_0}\frac{\partial\rho_0\overline{u'w'}}{\partial z}$, i.e., the gravity wave forcing, is ~201 m s^{-1} d^{-1}. The mean zonal wind U is mainly westward and has eastward shear in the vertical for both periods. In Period B, however, U is weaker above 86 km compared with that in Period A, and it is even eastward above 88 km. The change in U from Period A to Period B is ~15 m s^{-1} above 86 km. The sign of this tendency is consistent with the estimated gravity wave forcing, although the tendency is small compared to the zonal wave forcing. The large positive zonal wave forcing acts to accelerate the mean zonal wind, but the majority is balanced with the Coriolis force $-fV$ for the time scale much longer than a day in middle and high latitudes. Using ~201 m s^{-1} d^{-1} as the zonal wave forcing for Period A, V is estimated at ~17 m s^{-1}, which is consistent with observed V (Figure 8, top right).

As already indicated, an interesting feature is that V is stronger in Period B than in Period A, particularly around 88 km. In Period B, $U = 0$ around 88 km, and large momentum flux divergence which amounts to ~345 m s^{-1} d^{-1} is observed for the height range from 86.3 to 88.0 km. This strong zonal wind forcing is consistent with our inference that gravity waves increase which encounter their critical levels around 88 km following the descend of the $U = 0$ layer. By assuming that the zonal wave forcing is balanced with Coriolis force fV again, V is estimated at ~29.8 m s^{-1}, which roughly accords with the observation (Figure 8, bottom right).

It should be noted that the momentum flux divergence is not necessarily consistent with observed V in other height regions. For example, significant momentum flux divergence is not observed for a height region from 89 to 91 km in Period A or for 83.5–86 km for Period B, although large V is observed there. This inconsistency may be attributable to the wave forcing associated with other types of waves such as quasi-2 day waves and 5 day waves and other nonlinear contributors [e.g., *Becker*, 2012]. Note also that such planetary-scale waves can be generated by instability induced by gravity wave forcing in the mesosphere [*Sato and Nomoto*, 2015]. The momentum budget analysis including planetary-scale waves as well as gravity waves in the mesosphere and lower thermosphere based on observations is left for future studies.

A similar scenario was proposed by *Becker and Fritts* [2006] for the case of a major SSW in the SH in 2002. However, the two time periods analyzed in the present study may be slightly earlier than the potential response to the NH SSW, as already mentioned. It is also likely that the observed consistency between the temporal variations in U, V, and momentum flux convergence is related to internal variation in the SH. Nevertheless, this observed consistency confirms the effectiveness of MST radar observations for studies of mesospheric dynamics.

6. Summary and Concluding Remarks

Using continuous observations of the polar mesosphere summer echoes in a height region from 81 to 93 km performed by the PANSY radar, the first MST/IS radar in the Antarctic and located at Syowa Station (69.00°S, 39.35°E), over the three summer periods of 2013/2014, 2014/2015, and 2015/2016, statistical characteristics of wind fluctuations were examined. Spectral characteristics including w fluctuations and vertical flux of horizontal momentum were first elucidated over a wide-frequency range from (2π/8 min) to (2π/20 day) in the Antarctic mesosphere:

1. Power spectra of u and v (w) fluctuations obey a power law with an exponent of approximately -2 (-1) in the higher-frequency region than the inertial frequency f (corresponding to a period of 13 h) and have isolated peaks at approximately 1 day and a half day in the lower frequency region.
2. An isolated peak at an approximately 2 day period is observed in the horizontal wind spectra but is absent in the vertical wind spectra, which is consistent with previous studies' implication that the quasi-2 day waves are due to a normal-mode Rossby-gravity wave.

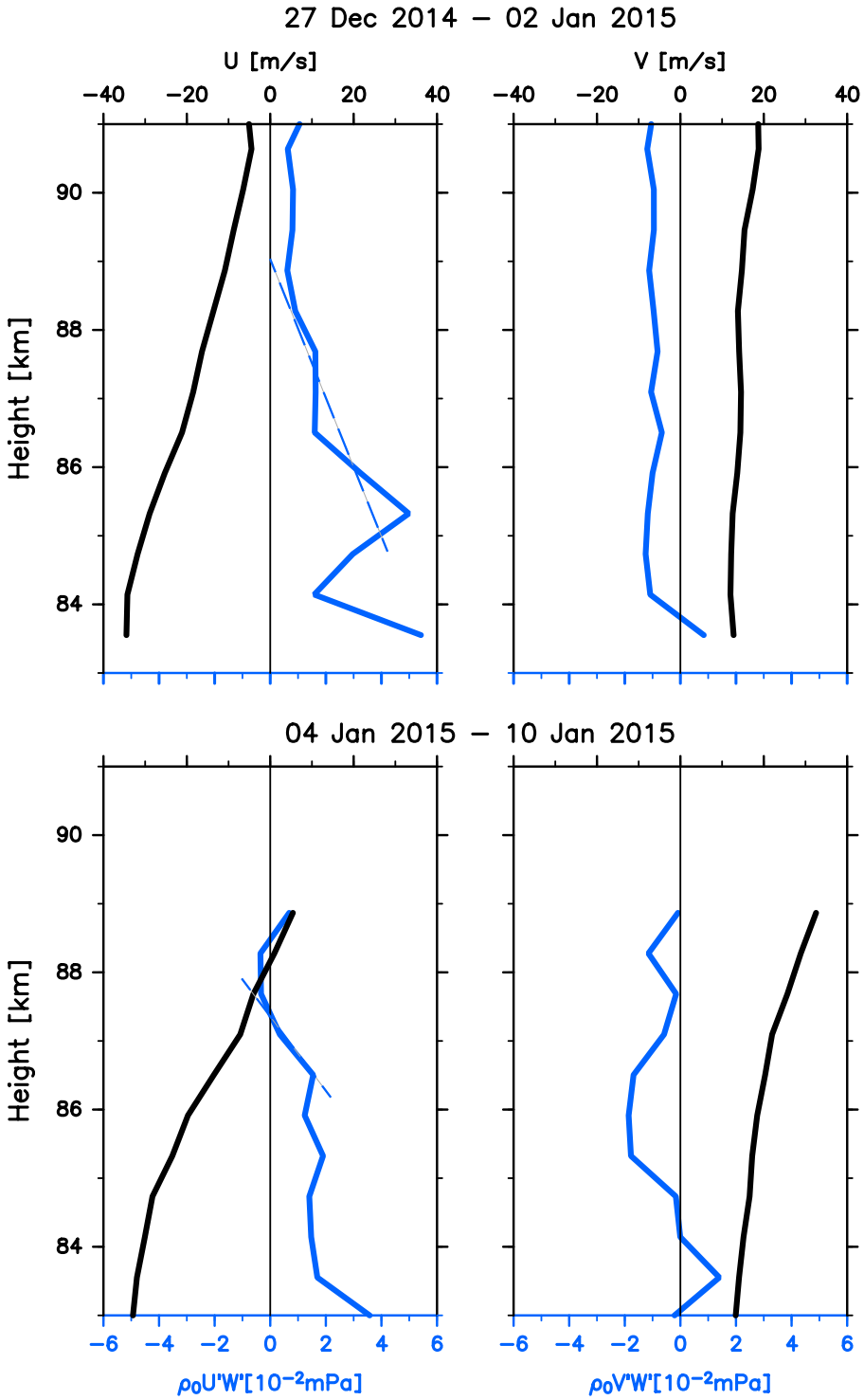

Figure 8. The same as Figure 6 but for the time periods of (top row) 27 December 2014 to 2 January 2015 and of (bottom row) 4–10 January 2015. Straight dashed lines on the left figures show the gradients used for the estimation of momentum flux divergence.

Note that spectral characteristics of such a wide-frequency range are rarely obtained using MST radars in low and middle latitudes because echoes from the mesosphere at nighttime are too weak to be detected. Ionization by continuous solar radiation all day long, in addition to the existence of polar mesospheric clouds in the Antarctic, allows us to observe continuous polar mesosphere summer echoes [*Rapp and Lübken*, 2003].

3. Vertical profiles of the time mean wind and momentum fluxes averaged over the whole PMSE season have significant year-to-year variation. It was seen that the momentum flux convergence $-\frac{1}{\rho_0}\frac{\partial \rho_0 \overline{u'w'}}{\partial z}$, which is regarded as the gravity wave forcing to the mean zonal wind, is largely positive where eastward shear of the westward mean wind is observed in the vertical.

Next, a case study was performed for 2014/2015 summer season when a minor SSW occurred in the NH on 3 January 2015. A significant momentum flux convergence corresponding to eastward acceleration of ~201 m s^{-1} d^{-1} was observed before the SSW onset. This gravity wave forcing is balanced with the Coriolis force associated with the mean equatorward wind. In 4–12 January 2015 after the onset, the westward mean zonal wind grew weaker and the level of $U = 0$ descends to 88 km, which is a consistent feature as an interhemispheric coupling signal initiated by the NH stratospheric warming. The gravity wave forcing got stronger around 88 km which amounts to ~345 m s^{-1} d^{-1}. Coincidently, the equatorward mean meridional wind grew stronger so as to keep the balance between the Coriolis force and gravity wave forcing. It is also worth noting that there are height regions where the Coriolis force associated with the equatorward flow does not accord with observed gravity wave forcing. This is likely due to other types of waves such as quasi-2 day and 5 day waves and other nonlinear contributors.

Given the unusual timing (i.e., quite early as a SH response to the NH SSW), this interesting change may not be related to the NH SSW. Instead, this change may be due to internal variation of the SH atmosphere. However, the observed systematic change in the momentum fluxes and the mean winds suggests that the MST radars in the polar region have the potential to examine changes in the mean field associated with gravity waves, including interhemispheric coupling associated with SSW. A combination of global MST radar network observations and gravity wave permitting general circulation model simulations [e.g., *Watanabe et al.*, 2008] is particularly promising to tackle the issue of the interhemispheric coupling through the mesosphere.

Acknowledgments
The authors thank the PANSY project members, Koji Nishimura, Yoshihiro Tomikawa, Taishi Hashimoto, and Takuji Nakamura. Thanks also to Erich Becker and two anonymous reviewers for their constructive comments. Figure 3 was drawn by Ryosuke Yasui using Aura MLS data. This work was supported by JSPS KAKENHI grants 25247075 and 16K17801 and by CREST, JST. PANSY is a multi-institutional project with a core of the University of Tokyo and National Institute of Polar Research, and the PANSY radar was operated by the Japanese Antarctic Research Expedition. The PANSY radar observation data are available at the project website, http://pansy.eps.s.u-tokyo.ac.jp.

References

Andrews, D. G., J. R. Holton, and C. B. Leovy (1987), *Middle Atmosphere Dynamics*, pp. 489, Academic Press, London.
Baumgaertner, A. J. G., A. J. McDonald, R. E. Hibbins, D. C. Fritts, D. J. Murphy, and R. A. Vincent (2008), Short-period planetary waves in the Antarctic middle atmosphere, *J. Atmos. Sol. Terr. Phys.*, *70*(10), 1336–1350, doi:10.1016/j.jastp.2008.04.007.
Becker, E. (2012), Dynamical control of the middle atmosphere, *Space Sci. Rev.*, *168*(1–4), 283–314, doi:10.1007/s11214-011-9841-5.
Becker, E., and S. Brune (2014), Reply to "Comments on 'Indications of Stratified Turbulence in a Mechanistic GCM'", *J. Atmos. Sci.*, *71*(2), 858–862, doi:10.1175/Jas-D-13-0281.1.
Becker, E., and D. C. Fritts (2006), Enhanced gravity-wave activity and interhemispheric coupling during the MaCWAVE/MIDAS northern summer program 2002, *Ann. Geophys.*, *24*(4), 1175–1188.
Becker, E., and G. Schmitz (2003), Climatological effects of orography and land-sea heating contrasts on the gravity wave-driven circulation of the mesosphere, *J. Atmos. Sci.*, *60*(1), 103–118, doi:10.1175/1520-0469(2003)060<0103:Ceooal>2.0.Co;2.
Becker, E., R. Knopfel, and F. J. Lübken (2015), Dynamically induced hemispheric differences in the seasonal cycle of the summer polar mesopause, *J. Atmos. Sol. Terr. Phys.*, *129*, 128–141, doi:10.1016/j.jastp.2015.04.014.
Blackman, R. B., and J. W. Tukey (1958), *The Measurement of Power Spectra from the Point of View of Communications Engineering*, Dover, New York.
Charney, J. G., and P. G. Drazin (1961), Propagation of planetary-scale disturbances from the lower into the upper atmosphere, *J. Geophys. Res.*, *66*(1), 83–109, doi:10.1029/JZ066i001p00083.
Chilson, P. B., E. Belova, M. T. Rietveld, S. Kirkwood, and U. P. Hoppe (2000), First artificially induced modulation of PMSE using the EISCAT heating facility, *Geophys. Res. Lett.*, *27*(23), 3801–3804, doi:10.1029/2000GL011897.
Cho, J. Y. N., and J. Röttger (1997), An updated review of polar mesosphere summer echoes: Observation, theory, and their relationship to noctilucent clouds and subvisible aerosols, *J. Geophys. Res.*, *102*(D2), 2001–2020, doi:10.1029/96JD02030.
Ecklund, W. L., and B. B. Balsley (1981), Long-term observations of the Arctic mesosphere with the MST radar at Poker Flat, Alaska, *J. Geophys. Res.*, *86*(Na9), 7775–7780, doi:10.1029/JA086ia09p07775.
Fukao, S., T. Sato, T. Tsuda, S. Kato, M. Inaba, and I. Kimura (1988), VHF Doppler radar determination of the momentum flux in the upper troposphere and lower stratosphere: Comparison between the three- and four-beam methods, *J. Atmos. Oceanic Technol.*, *5*(1), 57–69, doi:10.1175/1520-0426(1988)005<0057:vdrdot>2.0.co;2.
Guzman, A. E., J. May, H. Alvarez, and K. Maeda (2011), All-sky galactic radiation at 45 MHz and spectral index between 45 and 408 MHz, *Astron. Astrophys.*, *525*, A138, doi:10.1051/0004-6361/200913628.
Havnes, O. (2004), Polar Mesospheric Summer Echoes (PMSE) overshoot effect due to cycling of artificial electron heating, *J. Geophys. Res.*, *109*, A02309, doi:10.1029/2003JA010159.
Hoffmann, P., W. Singer, and J. Bremer (1999), Mean seasonal and diurnal variations of PMSE and winds from 4 years of radar observations at ALOMAR, *Geophys. Res. Lett.*, *26*(11), 1525–1528, doi:10.1029/1999GL900279.
Hoffmann, P., M. Rapp, J. Fiedler, and R. Latteck (2008), Influence of tides and gravity waves on layering processes in the polar summer mesopause region, *Ann. Geophys.*, *26*(12), 4013–4022.
Holton, J. R. (1983), The influence of gravity-wave breaking on the general-circulation of the middle atmosphere, *J. Atmos. Sci.*, *40*(10), 2497–2507, doi:10.1175/1520-0469(1983)040<2497:Tiogwb>2.0.Co;2.
Hosokawa, K., T. Ogawa, N. F. Arnold, M. Lester, N. Sato, and A. S. Yukimatu (2005), Extraction of polar mesosphere summer echoes from SuperDARN data, *Geophys. Res. Lett.*, *32*, L12801, doi:10.1029/2005GL022788.

Karlsson, B., C. E. Randall, S. Benze, M. Mills, V. L. Harvey, S. M. Bailey, and J. M. Russell (2009), Intra-seasonal variability of polar mesospheric clouds due to inter-hemispheric coupling, *Geophys. Res. Lett.*, *36*, L20802, doi:10.1029/2009GL040348.

Kassa, M., O. Havnes, and E. Belova (2005), The effect of electron bite-outs on artificial electron heating and the PMSE overshoot, *Ann. Geophys.*, *23*(12), 3633–3643.

Kirkwood, S., I. Wolf, H. Nilsson, P. Dalin, D. Mikhaylova, and E. Belova (2007), Polar mesosphere summer echoes at Wasa, Antarctica (73°S): First observations and comparison with 68°N, *Geophys. Res. Lett.*, *34*, L15803, doi:10.1029/2007GL030516.

Körnich, H., and E. Becker (2010), A simple model for the interhemispheric coupling of the middle atmosphere circulation, *Adv. Space Res.*, *45*(5), 661–668, doi:10.1016/j.asr.2009.11.001.

Latteck, R., W. Singer, R. J. Morris, D. A. Holdsworth, and D. J. Murphy (2007), Observation of polar mesosphere summer echoes with calibrated VHF radars at 69° in the Northern and Southern Hemispheres, *Geophys. Res. Lett.*, *34*, L14805, doi:10.1029/2007GL030032.

Lübken, F. J., J. Hoffner, T. P. Viehl, B. Kaifler, and R. J. Morris (2014), Winter/summer mesopause temperature transition at Davis (69°S) in 2011/2012, *Geophys. Res. Lett.*, *41*, 5233–5238, doi:10.1002/2014GL060777.

Lübken, F. J., R. Latteck, E. Becker, J. Hoffner, and D. Murphy (2016), Using polar mesosphere summer echoes and stratospheric/mesospheric winds to explain summer mesopause jumps in Antarctica, *J. Atmos. Sol. Terr. Phys.*, doi:10.1016/j.jastp.2016.06.008.

Manney, G. L., Z. D. Lawrence, M. L. Santee, W. G. Read, N. J. Livesey, A. Lambert, L. Froidevaux, H. C. Pumphrey, and M. J. Schwartz (2015), A minor sudden stratospheric warming with a major impact: Transport and polar processing in the 2014/2015 Arctic winter, *Geophys. Res. Lett.*, *42*, 7808–7816, doi:10.1002/2015GL065864.

Minamihara, Y., K. Sato, M. Kohma, and M. Tsutsumi (2016), Characteristics of vertical wind fluctuations in the lower troposphere at Syowa Station in the Antarctic revealed by the PANSY radar, *SOLA*, *12*, 116–120, doi:10.2151/sola.2016-026.

Miyahara, S., Y. Hayashi, and J. D. Mahlman (1986), Interactions between gravity-waves and planetary-scale flow simulated by the GFDL SKYHI general-circulation model, *J. Atmos. Sci.*, *43*(17), 1844–1861, doi:10.1175/1520-0469(1986)043<1844:Ibgwap>2.0.Co;2.

Morris, R. J., D. J. Murphy, I. M. Reid, D. A. Holdsworth, and R. A. Vincent (2004), First polar mesosphere summer echoes observed at Davis, Antarctica (68.6°S), *Geophys. Res. Lett.*, *31*, L16111, doi:10.1029/2004GL020352.

Muraoka, Y., S. Fukao, T. Sugiyama, M. Yamamoto, T. Nakamura, T. Tsuda, and S. Kato (1990), Frequency-spectra of mesospheric wind fluctuations observed with the MU radar, *Geophys. Res. Lett.*, *17*(11), 1897–1900, doi:10.1029/Gl017i011p01897.

Murphy, D. J., S. P. Alexander, and R. A. Vincent (2012), Interhemispheric dynamical coupling to the southern mesosphere and lower thermosphere, *J. Geophys. Res.*, *117*, D08114, doi:10.1029/2011JD016865.

Placke, M., P. Hoffmann, and M. Rapp (2015), First experimental verification of summertime mesospheric momentum balance based on radar wind measurements at 69A degrees N, *Ann. Geophys.*, *33*(9), 1091–1096, doi:10.5194/angeo-33-1091-2015.

Rapp, M., and F. J. Lübken (2000), Electron temperature control of PMSE, *Geophys. Res. Lett.*, *27*(20), 3285–3288, doi:10.1029/2000GL011922.

Rapp, M., and F. J. Lübken (2003), On the nature of PMSE: Electron diffusion in the vicinity of charged particles revisited, *J. Geophys. Res.*, *108*(D8), 8437, doi:10.1029/2002JD002857.

Rapp, M., and F. J. Lübken (2004), Polar mesosphere summer echoes (PMSE): Review of observations and current understanding, *Atmos. Chem. Phys.*, *4*, 2601–2633.

Rapp, M., I. Strelnikova, R. Latteck, P. Hoffmann, U. P. Hoppe, I. Haggstrom, and M. T. Rietveld (2008), Polar mesosphere summer echoes (PMSE) studied at Bragg wavelengths of 2.8 m, 67 cm, and 16 cm, *J. Atmos. Sol. Terr. Phys.*, *70*(7), 947–961, doi:10.1016/j.jastp.2007.11.005.

Rodgers, C. D., and A. J. Prata (1981), Evidence for a traveling two-day wave in the middle atmosphere, *J. Geophys. Res.*, *86*(C10), 9661–9664, doi:10.1029/JC086ic10p09661.

Salby, M. L. (1981), The 2-day wave in the middle atmosphere—Observations and theory, *J. Geophys. Res.*, *86*(Nc10), 9654–9660, doi:10.1029/JC086ic10p09654.

Sato, K. (1990), Vertical wind disturbances in the troposphere and lower stratosphere observed by the MU radar, *J. Atmos. Sci.*, *47*(23), 2803–2817, doi:10.1175/1520-0469(1990)047<2803:Vwditt>2.0.Co;2.

Sato, K. (2000), Sources of gravity waves in the polar middle atmosphere, *Adv. Polar Upper Atmos. Res.*, *14*, 233–240.

Sato, K., and M. Nomoto (2015), Gravity wave-induced anomalous potential vorticity gradient generating planetary waves in the winter mesosphere, *J. Atmos. Sci.*, *72*(9), 3609–3624, doi:10.1175/Jas-D-15-0046.1.

Sato, K., D. J. O'Sullivan, and T. J. Dunkerton (1997), Low-frequency inertia-gravity waves in the stratosphere revealed by three-week continuous observation with the MU radar, *Geophys. Res. Lett.*, *24*(14), 1739–1742, doi:10.1029/97GL01759.

Sato, K., T. Kumakura, and M. Takahashi (1999), Gravity waves appearing in a high-resolution GCM simulation, *J. Atmos. Sci.*, *56*(8), 1005–1018, doi:10.1175/1520-0469(1999)056<1005:Gwaiah>2.0.Co;2.

Sato, K., T. Kinoshita, and K. Okamoto (2013), A new method to estimate three-dimensional residual mean circulation in the middle atmosphere and its application to gravity-wave resolving general circulation model data, *J. Atmos. Sci.*, *70*(12), 3756–3779, doi:10.1175/jas-d-12-0352.1.

Sato, K., M. Tsutsumi, T. Sato, T. Nakamura, A. Saito, Y. Tomikawa, K. Nishimura, M. Kohma, H. Yamagishi, and T. Yamanouchi (2014), Program of the Antarctic Syowa MST/IS radar (PANSY), *J. Atmos. Sol. Terr. Phys.*, *118*, 2–15, doi:10.1016/j.jastp.2013.08.022.

Shibuya, R., K. Sato, Y. Tomikawa, M. Tsutsumi, and T. Sato (2015), A study of multiple tropopause structures caused by inertia-gravity waves in the Antarctic, *J. Atmos. Sci.*, *72*(5), 2109–2130, doi:10.1175/Jas-D-14-0228.1.

Smirnova, M., E. Belova, and S. Kirkwood (2012), Aspect sensitivity of polar mesosphere summer echoes based on ESRAD MST radar measurements in Kiruna, Sweden in 1997–2010, *Ann. Geophys.*, *30*(3), 457–465, doi:10.5194/angeo-30-457-2012.

Stober, G., S. Sommer, M. Rapp, and R. Latteck (2013), Investigation of gravity waves using horizontally resolved radial velocity measurements, *Atmos. Meas. Tech.*, *6*(10), 2893–2905, doi:10.5194/amt-6-2893-2013.

Strelnikova, I., and M. Rapp (2011), Majority of PMSE spectral widths at UHF and VHF are compatible with a single scattering mechanism, *J. Atmos. Sol. Terr. Phys.*, *73*(14–15), 2142–2152, doi:10.1016/j.jastp.2010.11.025.

Swarnalingam, N., W. K. Hocking, W. Singer, and R. Latteck (2009), Calibrated measurements of PMSE strengths at three different locations observed with SKiYMET radars and narrow beam VHF radars, *J. Atmos. Sol. Terr. Phys.*, *71*(17–18), 1807–1813, doi:10.1016/j.jastp.2009.06.014.

Tomikawa, Y., M. Nomoto, H. Miura, M. Tsutsumi, K. Nishimura, T. Nakamura, H. Yamagishi, T. Yamanouchi, T. Sato, and K. Sato (2015), Vertical wind disturbances during a strong wind event observed by the PANSY radar at Syowa Station, Antarctica, *Mon. Weather Rev.*, *143*(5), 1804–1821, doi:10.1175/Mwr-D-14-00289.1.

Tsuda, T., Y. Murayama, M. Yamamoto, S. Kato, and S. Fukao (1990), Seasonal-variation of momentum flux in the mesosphere observed with the MU radar, *Geophys. Res. Lett.*, *17*(6), 725–728, doi:10.1029/GL017i006p00725.

Varney, R. H., M. C. Kelley, M. J. Nicolls, C. J. Heinselman, and R. L. Collins (2011), The electron density dependence of polar mesospheric summer echoes, *J. Atmos. Sol. Terr. Phys.*, *73*(14–15), 2153–2165, doi:10.1016/j.jastp.2010.07.020.

Vincent, R. A., and I. M. Reid (1983), HF Doppler measurements of mesospheric gravity-wave momentum fluxes, *J. Atmos. Sci.*, *40*(5), 1321–1333, doi:10.1175/1520-0469(1983)040<1321:Hdmomg>2.0.Co;2.

Watanabe, S., Y. Kawatani, Y. Tomikawa, K. Miyazaki, M. Takahashi, and K. Sato (2008), General Aspects of a T213L256 Middle Atmosphere General Circulation Model, *J. Geophys. Res.*, *113*, D12110, doi:10.1029/2008JD010026.

Waters, J. W., et al. (2006), The Earth observing system Microwave Limb Sounder (EOS MLS) on the Aura satellite, *IEEE Trans. Geosci. Remote Sens.*, *44*(5), 1075–1092, doi:10.1109/Tgrs.2006.873771.

Woodman, R. F., B. B. Balsley, F. Aquino, L. Flores, E. Vazquez, M. Sarango, M. M. Huaman, and H. Soldi (1999), First observations of polar mesosphere summer echoes in Antarctica, *J. Geophys. Res.*, *104*(A10), 22,577–22,590, doi:10.1029/1999JA900226.

Yasuda, Y., K. Sato, and N. Sugimoto (2015a), A theoretical study on the spontaneous radiation of inertia-gravity waves using the renormalization group method. Part I: Derivation of the renormalization group equations, *J. Atmos. Sci.*, *72*(3), 957–983, doi:10.1175/Jas-D-13-0370.1.

Yasuda, Y., K. Sato, and N. Sugimoto (2015b), A theoretical study on the spontaneous radiation of inertia-gravity waves using the renormalization group method. Part II: Verification of the theoretical equations by numerical simulation, *J. Atmos. Sci.*, *72*(3), 984–1009, doi:10.1175/Jas-D-13-0371.1.

Yasui, R., K. Sato, and M. Tsutsumi (2016), Seasonal and interannual variation of mesospheric gravity waves based on MF radar observations over 15 years at Syowa Station in the Antarctic, *SOLA*, *12*, 46–50, doi:10.2151/sola.2016-010.